

X-ray emission associated with radiative recombination for Pb⁸²⁺ ions at threshold energies

B. Zhu^{1,2,3,4,*}, A. Gumberidze², T. Over³, G. Weber^{1,2}, Z. Andelkovic², A. Bräuning-Demian², R. J. Chen^{2,5}, D. Dmytriiev², O. Forstner^{1,2,3}, C. Hahn^{1,2,3}, F. Herfurth², M. O. Herdrich^{1,2,3}, P.-M. Hillenbrand^{2,6}, A. Kalinin², F. M. Kröger^{1,2,3}, M. Lestinsky², Yu. A. Litvinov², E. B. Menz^{1,2,3}, W. Middents^{1,2,3}, T. Morgenroth^{1,2,3}, N. Petridis², Ph. Pfäfflein^{1,2,3}, M. S. Sanjari^{2,7}, R. S. Sidhu², U. Spillmann², R. Schuch⁸, S. Schippers^{6,9}, S. Trotsenko^{1,2}, L. Varga², G. Vorobyev² and Th. Stöhlker^{1,2,3,†}

¹Helmholtz Institute Jena, D-07743 Jena, Germany

²GSI Helmholtzzentrum für Schwerionenforschung GmbH, D-64291 Darmstadt, Germany

³Institut für Optik und Quantenelektronik, Friedrich-Schiller-Universität Jena, D-07743 Jena, Germany

⁴School of Nuclear Science and Technology, Lanzhou University, Lanzhou 730000, China

⁵Institute of Modern Physics, Chinese Academy of Sciences, Lanzhou 730000, China

⁶I. Physikalisches Institut, Justus-Liebig-Universität Gießen, D-35392 Giessen, Germany

⁷Department of Chemistry and Biotechnology, Aachen University of Applied Sciences, D-52005 Aachen, Germany

⁸Physics Department, Stockholm University, S-106 91 Stockholm, Sweden

⁹Helmholtz Research Academy Hesse for FAIR (HFHF), Campus Gießen, D-35392 Giessen, Germany



(Received 19 January 2022; accepted 31 March 2022; published 10 May 2022)

For decelerated bare lead ions at a low beam energy of 10 MeV/u, the x-ray emission associated with radiative recombination (RR) at threshold energies has been studied at the electron cooler of CRYRING@ESR at GSI, Darmstadt. In our experiment, we observed the full x-ray emission pattern by utilizing dedicated x-ray detection chambers installed at 0° and 180° observation geometry. Most remarkably, no line distortion effects due to delayed emission are present in the well-defined x-ray spectra, spanning a wide range of x-ray energies (from about 5 to 100 keV), which enables us to identify fine-structure resolved Lyman, Balmer, and Paschen x-ray lines along with the RR transitions into the *K*, *L*, and *M* shells of the ions. For comparison with theory, an elaborate theoretical model is established taking into account the initial population distribution via RR for all atomic levels up to Rydberg states with principal quantum number $n = 165$ in combination with time-dependent feeding transitions. Within the statistical accuracy, the experimental data are in very good agreement with the results of rigorous relativistic predictions. Most notably, this comparison sheds light on the contribution of prompt and delayed x-ray emission (up to 70 ns) to the observed x-ray spectra, originating in particular from yrast transitions into inner shells.

DOI: [10.1103/PhysRevA.105.052804](https://doi.org/10.1103/PhysRevA.105.052804)

I. INTRODUCTION

Radiative recombination (RR), the time reversal of photoionization, can be considered one of the most elementary and fundamental atomic processes and is the major recombination process occurring for electron beams and bare ions. In particular, it is of utmost importance for matter in highly ionized plasma states, such as those prevalent in stars. In this process, a free electron recombines into a bound state of an ion via the emission of a photon, carrying away the difference in energy between the initial (continuum) and final (bound) electronic states and satisfying momentum conservation.

For low relative energies, the first measurements of the RR process were done in merged-beam geometry utilizing ion and electron beams [1,2]. Further detailed experimental studies of this process for low- to mid-*Z* ions in various electronic configurations [3–7] and even many-electron ions at high *Z* [8,9] have been facilitated, in particular, by the advancement of ion storage rings employing electron-cooler devices (such as ASTRID [10], CRYRING [11], and TSR [12]). For the heaviest ion species these studies were extended at the electron cooler of the ESR ion storage ring [13–16]. Moreover, at high relative collision energies, complementary studies have been performed at electron-beam ion-trap devices [17,18]. For completeness we would like to add that very extensive and detailed information about the closely related process of radiative electron capture occurring in ion-atom collisions has been obtained for a broad range of ion species and collision energies up to ultrarelativistic collision conditions [19].

Theoretically, the RR process has been exhaustively investigated, first with a semiclassical approach [20] and then more rigorously with quantum mechanics [21], and can be treated nowadays in a fully relativistic fashion for

*binghui.zhu@uni-jena.de

†t.stoehlker@gsi.de

Published by the American Physical Society under the terms of the [Creative Commons Attribution 4.0 International license](https://creativecommons.org/licenses/by/4.0/). Further distribution of this work must maintain attribution to the author(s) and the published article's title, journal citation, and DOI.

initially bare ions [22–24], whereas for many-electron systems very accurate many-body approaches are also available [25,26]. Furthermore, recently, even quantum electrodynamics (QED) contributions have been taken into account in the description of the RR process [27,28]. RR has been studied quite intensively over decades, and many interesting insights have been gained into various aspects of this process, such as polarization properties of emitted x-ray photons [29,30] and angular-distribution-related spin-flip identifications [31,32]. However, a strong enhancement of electron-ion recombination-rate coefficients at sub-eV relative energies observed at electron-cooler devices is not yet fully understood for highly charged ions [5,7,13,14,16,33] and deserves further investigations from both experiment and theory.

In most of the RR experiments (performed at electron coolers of ion storage rings), total recombination rates have been measured as a function of the relative energy between electrons and ions. In addition to those, measurements have been performed at the ESR where x-ray emission due to the RR process in the electron cooler has been observed [15,16,34–36]. These measurements have provided detailed insights into the state-selective population dynamics of the RR and the subsequent cascade processes. Moreover, x-ray spectroscopy at the ESR electron cooler has proven to be a powerful tool to precisely measure binding energies in the heaviest hydrogen- and heliumlike ions and thus to gain access to QED effects in the regime of strong fields [34,36–38]. Here, we would like to note that in heavy highly charged ions the parameter $v/c \sim \alpha Z$ (α is the fine-structure constant, and v is the electron velocity on the ground state) is comparable to unity. Therefore, their basic atomic characteristics, such as energy levels and transition probabilities, are strongly influenced by relativistic or even QED effects. This often leads to new spectral patterns that are remarkably different from the spectra of light elements [39]. To be more specific, the forbidden radiative transitions (such as $M1$, $M2$, $E2$) are enhanced by 2–6 orders of magnitude [40,41] relative to the allowed $E1$ transition, which scales approximately as Z^4 .

Recently, CRYRING was transferred from the Manne Siegbahn Laboratory in Stockholm to GSI/FAIR in Darmstadt and was installed behind the ESR storage ring as an in-kind contribution from Sweden to the upcoming international facility for Antiproton and Ion Research (FAIR) (see [42] and references therein). At Stockholm, CRYRING has provided pioneering results over many years [6–9] and was recently further optimized for future experiments with heavy bare and few-electron ions, exotic nuclei, and antiprotons at FAIR [43]. At FAIR, CRYRING@ESR is an important part of a portfolio for trapping and storage facilities for cooled highly charged heavy ions bridging an energy range over more than 10 orders of magnitude, spanning from rest in the laboratory up to highly relativistic energies [44]. In combination with the ESR storage ring, CRYRING offers unique opportunities for a broad range of experiments with the heaviest electron-cooled one- and few-electron ions at low energies [45]. At CRYRING@ESR one can store ions at low beam energies (typically below 15 MeV/u), far below the production energy required to produce the desired charge state of interest; for example, the efficient production of Pb^{82+} requires energies of at least 300 MeV/u. Another unique selling point of

CRYRING@ESR is the adiabatic expansion of the electron beam [46,47], resulting in an up to 100 times lower transverse electron temperature compared to ESR. Since 2020, the so-called CRYRING@ESR facility has been fully commissioned with beams both from the local ion injector and from the ESR storage ring and is now available for the first physics production runs.

In this paper, we report on an x-ray spectroscopy study associated with the RR process for bare lead ions at the electron cooler of the CRYRING@ESR storage ring. For this purpose, decelerated 10-MeV/u lead ions and 0° and 180° observation geometry were applied. Most noticeably, at 0° x-ray emission lines were observed without any line distortion effects caused by delayed x-ray emission affecting, in particular, the Lyman series [34–36,38]. Moreover, for the experiment we used beryllium foils for vacuum separation from the 10^{-11} -mbar UHV environment of CRYRING@ESR to the x-ray detectors, which enabled us to observe the full, well-resolved emission pattern ranging from the Paschen series up to the K -RR line under almost-background-free conditions. These very clean x-ray spectra allow for a detailed comparison of the observed full photon emission pattern with theoretical x-ray spectrum modeling based on elaborate calculations of the RR process, taking into consideration feeding cascades. As a consequence, the interpretation of relative intensities of fine-structure-resolved characteristic x rays is performed by comparison with rigorous relativistic calculations. These detailed studies pave the way for a refined understanding of the level population under such exotic collision conditions and may help us to investigate the issue of the rate enhancement for recombination in electron-cooler devices. All in all, the current experiment can be considered a prerequisite for future precision x-ray spectroscopy studies at the electron cooler of CRYRING@ESR; such experiments are currently planned within the SPARC collaboration [48] with the aim to test atomic-structure theory and QED effects in strong fields close to the Schwinger limit with unprecedented precision by utilizing, e.g., novel high-resolution microcalorimeters [49,50].

II. THE EXPERIMENT

For the experiment performed in May 2020, about 10^7 isotope clean $^{208}\text{Pb}^{82+}$ ions from the UNILAC/SIS accelerator complex were injected into the ESR at the specific energy of 400 MeV/u. The stored ions were efficiently stochastically cooled at this injection energy as well as by Coulomb interaction with the cold comoving electrons [51] in the ESR electron cooler. Thereafter, the ions were decelerated down to 10 MeV/u and electron cooled again, followed by their extraction out of the ESR and injection into the CRYRING@ESR. After these steps, $\sim 10^5$ Pb^{82+} ions were usually stored in the CRYRING@ESR. In order to guarantee a well-defined constant beam velocity, generally of the order of $\Delta\beta/\beta \sim 10^{-5}$, electron currents of, typically, 10 to 20 mA were applied at the CRYRING@ESR cooler. Moreover, the electron cooling provides a small beam size with a typical diameter of 2 mm, a reduced relative momentum spread $\Delta p/p \sim 10^{-5}$, and an emittance of the ion beam of less than 0.1π mm mrad.

The experimental setup for the measurement of x-ray radiation at the electron cooler of the CRYRING@ESR is shown

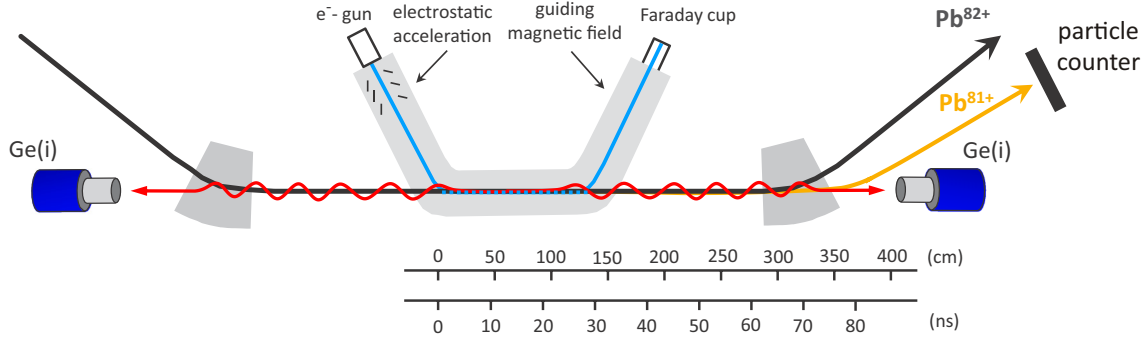


FIG. 1. Experimental setup at the electron cooler of the CRYRING@ESR storage ring. The x-ray emission from the electron-ion beam interaction region is viewed at 0° and 180° by Ge(i) detectors. X rays are measured in coincidence with down-charged Pb^{81+} projectiles detected by the particle counter installed behind the electron cooler. A length scale and a timescale, valid for a beam velocity of $\beta \approx 0.146$ (10 MeV/u), are shown at the bottom. Note that the time of flight of the ions passing the cooler section is close to 30 ns, whereas the time of flight of ions from the entrance of the cooler section up to the end of the straight section amounts to 70 ns.

in Fig. 1. At the electron cooler dedicated vacuum separation chambers were used [52], equipped with beryllium view ports allowing for x-ray detection under 0° and 180° with respect to the ion-beam axis. The exact geometry of the whole detector arrangement was precisely determined by laser-assisted trigonometry. The x-ray detection was accomplished by two high-purity, planar germanium x-ray detectors, which were mounted 3.5 m at 0° and 3.3 m at 180° with regard to the midpoint of the roughly 1.2-m-long straight electron-cooler section. The detector at 0° had a crystal diameter of 16 mm (crystal thickness of 10 mm) and was equipped with an x-ray collimator (10 mm thick, made out of brass and reducing the effective detector area to 79 mm^2). This results in a solid-angle coverage of $\Delta\Omega/\Omega$ which varies along the cooler section from $\approx 6.3 \times 10^{-7}$ to $\approx 1.3 \times 10^{-6}$. At 180° the detector used had a diameter of 49.7 mm (crystal thickness of 21 mm) and was equipped with an x-ray collimator (10 mm thick, made out of brass and reducing the effective detector area to 962 mm^2). There $\Delta\Omega/\Omega$ varies along the cooler section ranging from $\approx 1.0 \times 10^{-5}$ to $\approx 4.9 \times 10^{-6}$. In addition, due to the relativistic solid-angle transformation, the effective solid angle at 0° observation angle for photons being emitted in the rest frame of the ions is enhanced relative to the one at 180° by a factor of 1.8. In order to suppress the dominant background, stemming from x-ray emission (bremsstrahlung) by a fraction of the electron beam hitting materials in the cooler [53] and from natural radioactivity, an ion detector based on secondary electron detection (channel electron multiplier) was operated downstream to the cooler [54]. The coincidences between the x rays from the interaction region of the electron cooler and the down-charged Pb^{81+} ions allowed for the unambiguous identification of those x rays associated with radiative recombination events.

In the present experiment where recombination of free electrons at zero relative electron-ion velocity on average is studied, high Rydberg states of the ions are expected to be populated [15,16,34–36,55]. The ions in these highly excited states might be reionized when exposed to magnetic field of the next dipole magnet of CRYRING@ESR on their way to the particle detector. The highest n_{dip} state that survives field ionization, defined by the dipole magnet setting of the storage

ring [56], is usually estimated by the formula [57,58]

$$n_{\text{dip}} = (6.2 \times 10^{10} q^3 / v_i B)^{1/4}, \quad (1)$$

where q is the charge state, v_i is the ion-beam velocity, and B is the magnetic-field strength in teslas. In this experiment, n_{dip} is estimated to be 165, corresponding to a magnetic rigidity value of 1.17 Tm of the dipole magnet. We note that rather sophisticated and detailed studies on the reionization of highly excited states in magnetic fields were reported in [59–61], pointing out the relevance of Rydberg states with an even higher main quantum number n [larger than the one defined by Eq. (1)] but with low orbital quantum number l which are not field ionized and thus could still contribute to the observed rate in the particle detector. Indeed, even in our current experiment related cascade transitions could be possible during the flight time of ions to the dipole magnet. However, as discussed below, these states are not significantly populated via RR (see Fig. 4 below) and will be neglected in the following.

The three-body recombination process in the cooler can lead to the population of states with binding energies comparable to an electron-beam temperature [62,63] of a few meV. For H-like lead ions, this corresponds to a Rydberg state with $n \approx 4000$. Since this value is far beyond n_{dip} and the corresponding radiative lifetime is orders of magnitude larger than the flight time of ions from the center of the cooling section to the dipole magnet, the three-body recombination process will hardly contribute to the observed x-ray intensities [35].

Although in this experiment with bare high- Z ions at CRYRING@ESR only a low intensity of $\sim 10^5$ ions per injection could be achieved, a few days of continuous operation were sufficient to accumulate meaningful coincident x-ray spectra. Here, the experimental study benefits from the low ion-beam energy of 10 MeV/u. At this ion-beam energy, the energy as well as the intensity of bremsstrahlung caused by the cooler electrons is strongly reduced due to the comparably small cooler voltage of about 5.5 kV and a current of 12 mA (the maximum energy of the bremsstrahlung is given by the electron-cooler voltage applied). In this case, as one expects, bremsstrahlung will hardly contribute to the coincident (random events subtracted) x-ray spectra. Consequently, very clean conditions for x-ray spectroscopy were present at the

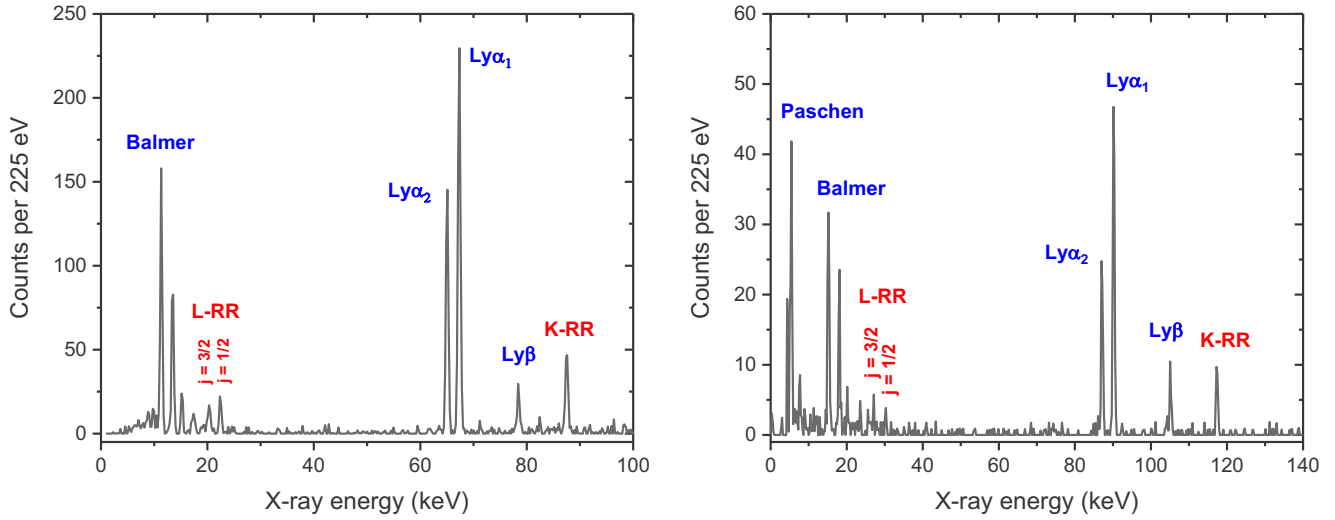


FIG. 2. X-ray spectra measured at observation angles of 180° (left) and 0° (right) by the two Ge(i) detectors in coincidence with 10 MeV/u Pb^{81+} projectiles detected after the electron cooler of the CRYRING@ESR storage ring. X-ray energies are given in the laboratory frame.

cooler. Also, our investigation profits from the 0° and 180° geometry of the x-ray detector setup, where Doppler broadening and possible uncertainties of the observation angles basically do not affect the observed x-ray spectra [38]. The result is depicted in Fig. 2, where the coincident x-ray spectra are plotted as observed for initially bare lead ions at an energy of 10 MeV/u. The energy scale of the spectra was calibrated during the measurement with γ lines of known energies from standard radioactive calibration sources of ^{241}Am , ^{133}Ba , and ^{57}Co , regularly placed in front of the detectors during the experiment.

To shed more light (in a qualitative manner) on the observation geometry, the extended size of the electron-cooler section, and the importance of delayed x-ray emission, we display in Fig. 3 a two-dimensional presentation of the coincidence time Δt versus the x-ray energy as observed at

0° . In Fig. 3 Δt refers to the time difference between photon (start) and particle (stop) detections (relative timescale) and can therefore be interpreted as a time-of-flight spectrum for the x-ray-emitting ions (note that the delayed emission is here at earlier times). Moreover, in contrast to the x-ray spectra shown before, this two-dimensional spectrum refers to all x-ray events registered in coincidence with the particle detector without any background subtraction applied (which is basically not present for energies above 5 keV). Therefore, random events caused by bremsstrahlung arising from the cooler section can be identified as a continuous, broad band at an energy close to 5 keV. In Fig. 3 we concentrate on purpose on the 0° detector because of its superior timing characteristics which exhibit a time resolution of ≈ 20 ns for energies above 30 keV. Although the spectrum displayed is hampered by statistics, clear line structures are visible that correspond

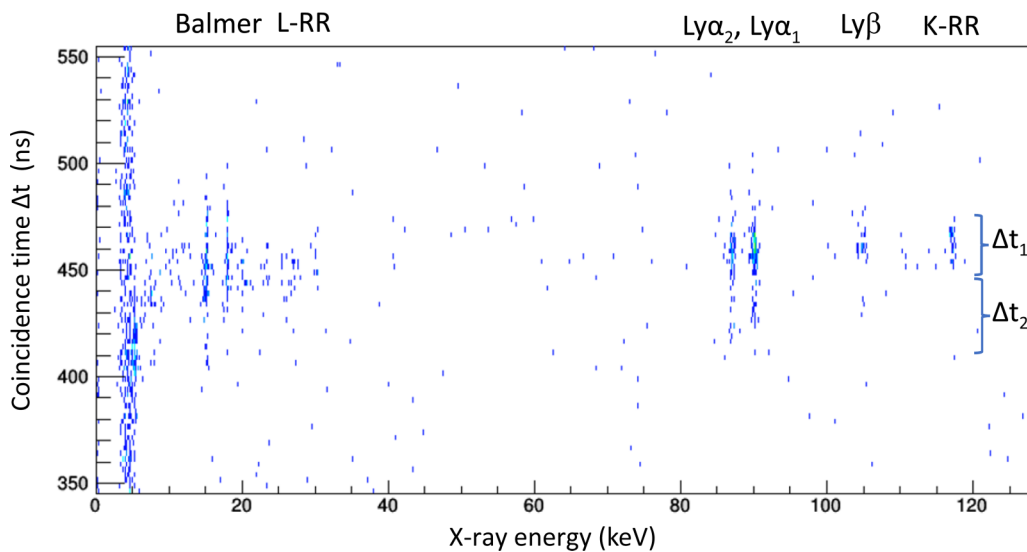


FIG. 3. Two-dimensional presentation of the coincidence time Δt versus the x-ray emission observed at 0° (laboratory frame). The coincidence time refers to the time difference between photon (start) and particle (stop) detections (relative timescale). $\Delta t_1 \approx 30$ ns refers to the cooler section; $\Delta t_2 \approx 40$ ns refers to the region outside the electron cooler.

to the line identification shown in Fig. 2 (see also the labels in Fig. 3). Most remarkably, the K -RR radiation, which can arise only from the cooler section of CRYRING@ESR, is distributed over a time interval of about $\Delta t_1 \approx 30$ ns, whereas the characteristic radiation (e.g., the Ly- α emission) is distributed over a time interval of $\Delta t_1 + \Delta t_2 \approx 70$ ns (Δt_1 refers to the cooler section; Δt_2 refers to the straight line outside the electron cooler), enabling clear identification of the x-ray emission occurring outside of the electron-cooler region. Considering the estimated flight times for ions inside and outside of the cooler section (see Fig. 1), very good agreement with the experimental findings can be stated. We would like to emphasize that our considerations refer to x-ray energies above 30 keV. Below 30 keV the time response of the x-ray detector deteriorates due to the reduction of the signal-to-noise ratio. However, extended line structures for the characteristic radiation are clearly visible for the Balmer region too.

In this context, it is interesting to compare our results with the situation at the ESR storage ring. In contrast to CRYRING@ESR with its exact 0° and 180° observation geometry, at the ESR electron cooler the x-ray detectors view the cooler section via thin stainless-steel foils at observation angles of close to 0.5° and 179.5° with respect to the ion-beam axis [15,16]. As a result, distinctive tails of Ly- α transition lines are observed at the ESR but not at CRYRING@ESR. At the ESR, these tails are caused by the delayed Ly- α emission which occurs at different positions and thus at different angles with respect to the x-ray detector (since the detector is not exactly on the beam axis) [15,38].

III. THEORETICAL BACKGROUND

In the experiment free electrons are captured via RR into the bare lead ions, populating excited levels of H-like lead which subsequently leads to photon emission by means of deexcitation transitions. Thus, the interpretation of the corresponding x-ray spectra requires accurate modeling of the RR process at electron-cooling conditions based on the integration over the relevant transverse and longitudinal velocity distributions between the ions and the electrons and at the same time performing appropriate calculations of RR for all relevant levels of the ions and therefore considering accurate binding energies and transition rates.

A. Relevant cross sections and rate coefficients

The theoretical description of RR is based on considering it the time reversal of the atomic photoelectric effect. For high- Z ions, such as H-like lead, it has been shown that for low-lying bound states, fully relativistic calculations are necessary to describe the RR process [19,64]. Therefore, in this work, we use complete relativistic calculations for RR into quantum states with $n \leq 10$. The exact evaluation of the relativistic photoelectric cross sections requires a partial-wave expansion of the Coulomb-Dirac continuum function. This means that closed-form expressions can no longer be derived, and one has to resort to numerical methods [19]. The numerical evaluation of the RR cross sections in strongly bound projectile states was performed in a fully relativistic manner following the detailed formulations in Refs. [23,65,66]. The accuracy

of the calculation is mainly determined by the number of expanded partial waves, $\nu = 2\kappa_{\max}$, with κ_{\max} being the maximum quantum number of the Dirac angular momentum. For the expansion, a too small choice of κ_{\max} may lead to truncation errors, whereas a too large value may lead to an explosion of numerical errors due to rapid oscillations of the radial part of the continuum wave function. In our calculations, all multipoles of the electron-photon interaction under inclusion of retardation effects are taken into account.

For the higher excited states with the main quantum number $n > 10$ we use the nonrelativistic dipole approximation [21,67]. In particular, we made use of a set of recurrence relations proposed by Burgess [68,69] (for a detailed discussion see [19]), allowing one to successively calculate all dipole matrix elements for a given electron kinetic energy, which has the advantage of being numerically stable and applicable for arbitrary (n, l) shells [70].

The electrons in the beam have a nonisotropic velocity distribution $f(\mathbf{v})$ in the rest frame of the ions in the cooler setup of a storage ring. In the experiment at the cooler one cannot measure the cross section σ_{nl} directly and instead measures the so-called rate coefficient α_{nl} , which is a product of σ_{nl} and the relative electron-ion velocity folded with $f(\mathbf{v})$:

$$\alpha_{nl} = \langle v\sigma_{nl}(\mathbf{v}) \rangle = \int v\sigma_{nl}(\mathbf{v})f(\mathbf{v})d^3v. \quad (2)$$

The measured α_{nl} can then be compared with the one from theoretically calculated σ_{nl} and a modeled $f(\mathbf{v})$, usually described in terms of an anisotropic Maxwell-Boltzmann distribution [46,71], characterized by effective longitudinal kT_{\parallel} and transverse kT_{\perp} beam temperatures (usually in eV):

$$f(\mathbf{v}) = \left(\frac{m_e}{2\pi}\right)^{3/2} \frac{1}{kT_{\perp}(kT_{\parallel})^{1/2}} \exp\left[-\left(\frac{m_e v_{\perp}^2}{2kT_{\perp}} + \frac{m_e v_{\parallel}^2}{2kT_{\parallel}}\right)\right], \quad (3)$$

where k is the Boltzmann constant and m_e is the electron mass.

Throughout, in the following, electron-beam temperatures of $kT_{\perp} \approx 2.59$ meV and $kT_{\parallel} \approx 51.8$ μ eV are used for the CRYRING@ESR cooler. These values were derived from a previous dielectronic-recombination experiment with lithium-like Ne^{7+} ions [72] in which the overall uncertainties can be estimated to be of the order of 10%. These numbers are found to be consistent with former temperature values obtained in experiments at CRYRING in Stockholm [73,74]. Figure 4 depicts the calculated state-selective total rate coefficients for RR into bare lead projectiles at the electron cooler of CRYRING@ESR as a function of the principal and angular momentum quantum numbers (n, l) . As can be seen, due to the small relative velocity between the electrons and the ions, the RR rate coefficient decreases only slightly with increasing principle quantum number n ($\alpha_{nl} \sim 1/n$) [75]. For completeness we note that for high Rydberg states with binding energies $E_B < kT_{\perp}$ the scaling law for RR at high relative energies is restored again ($\alpha_{nl} \sim 1/n^3$) [76]. Correspondingly, there are very significant contributions from high (n, l) levels regarding the production of characteristic projectile x rays resulting via radiative cascades from these high Rydberg levels [15,55].

In order to describe our experimental data, angular differential RR rate coefficients are needed since the electron

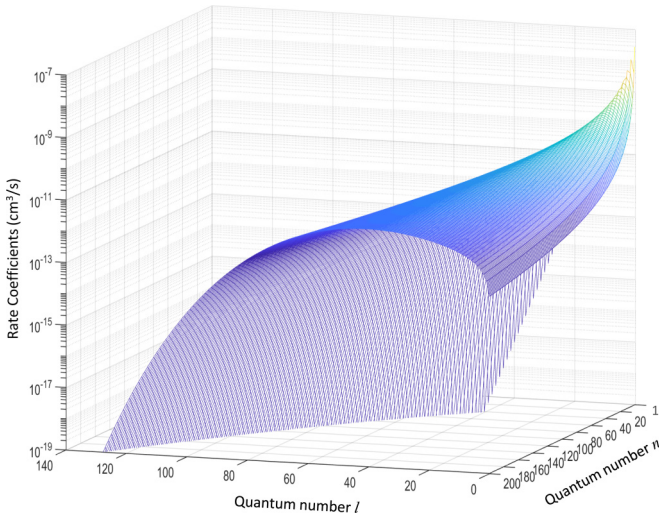


FIG. 4. State-selective rate coefficients α_{nl} calculated for RR into bare lead ions for the flattened electron velocity distribution with $kT_{\perp} = 2.59$ meV and $kT_{\parallel} = 51.8$ μ eV at the CRYRING@ESR electron cooler. A relativistic description of the RR process for inner shells up to $n = 10$ is considered here, whereas for higher shells the nonrelativistic dipole approximation is applied.

velocity distribution is nonisotropic in the rest frame of the ion and our x-ray detectors are placed at specific observation angles (0° and 180° with respect to the ion-beam direction). We performed relativistic calculations of the differential RR cross sections for the inner shells based on the technique discussed in detail by Eichler and colleagues [19,22,31,77] in order to describe the observed direct RR transitions into the K , L , and M shells of the ions. As an example, we show in Fig. 5 the angular differential cross sections for RR into the K and L shells of initially bare lead ions. In the particular case of the RR process occurring in the electron cooler, the transverse temperature ($kT_{\perp} = 2.59$ meV) of the electron beam is

much larger than the longitudinal one ($kT_{\parallel} = 51.8$ μ eV), and thus, the collision axis is defined as the one perpendicular to the ion-beam axis. Correspondingly, the calculated RR rate coefficients at 90° are used to compare our results with the experimental data registered by the two x-ray detectors mounted at 0° and 180° along the ion-beam axis. Here, it is important to stress that the shape of the RR angular distribution remains largely unchanged for the whole low-collision energy range defined by the temperatures of the electron beam in the electron cooler [19].

As already mentioned, at collision energies of a few meV because they prevail at the electron cooler of CRYRING@ESR, recombination into high Rydberg states and following radiative cascades will contribute significantly to the intensity of the characteristic radiation [15,34,35] (see also Fig. 4). This will substantially attenuate any potential initial alignment of excited states produced via RR which finally populate the states of the L and M shells via radiative cascades. Therefore, in contrast to the prompt RR radiation, we assume an isotropic emission pattern in the projectile frame for the subsequent characteristic projectile transitions of the observed Lyman, Balmer, and Paschen series [76,78].

B. Transition energies and probabilities

Since no existing database can provide the required extensive set of energy levels and radiative transition rates up to $n = 165$ for the relevant ions of lead, the input data for modeling the observed x-ray spectra need to be generated using an accurate atomic code. The Flexible Atomic Code (FAC) developed by Gu [79,80] based on the relativistic configuration interaction method with independent-particle base wave functions was used to generate the required atomic data, in which QED corrections are treated as hydrogenic approximations for self-energy and vacuum polarization effects. For H-like lead ions, the comparison of energy levels obtained from FAC code with the results from Johnson and

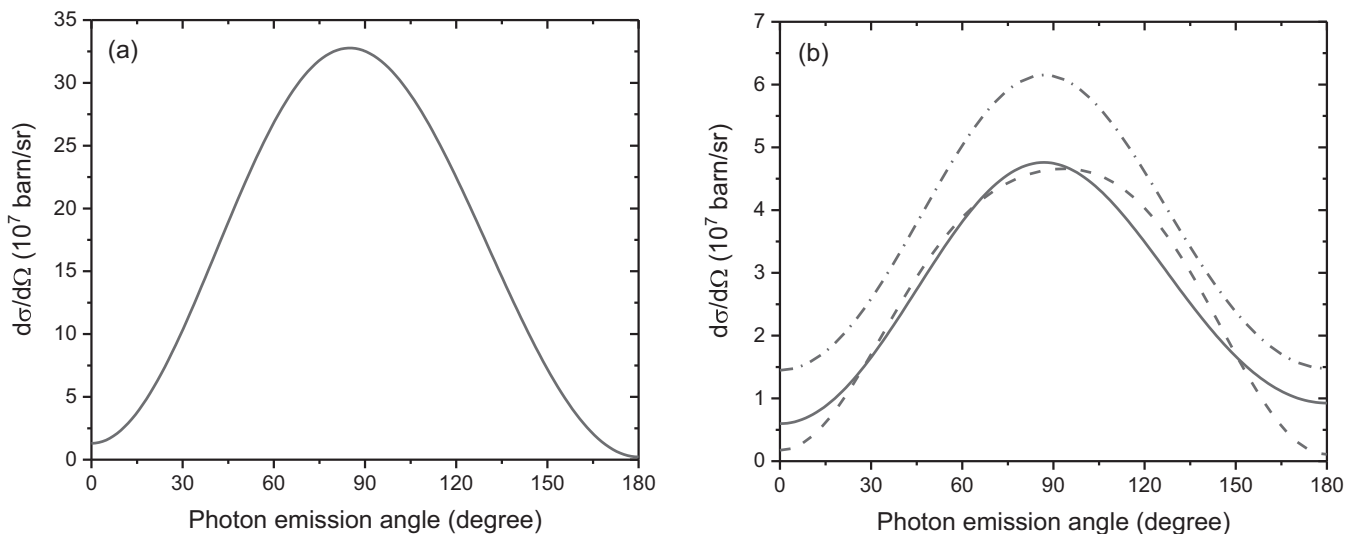


FIG. 5. Differential cross sections per vacancy calculated within the framework of the rigorous relativistic theory applied for RR of free electrons with bare lead ions at a relative electron-ion energy of 2.59 meV. (a) For the K shell and (b) for the various levels of the L shell (solid line: $2p_{3/2}$; dash-dotted line: $2p_{1/2}$; dashed line: $2s_{1/2}$).

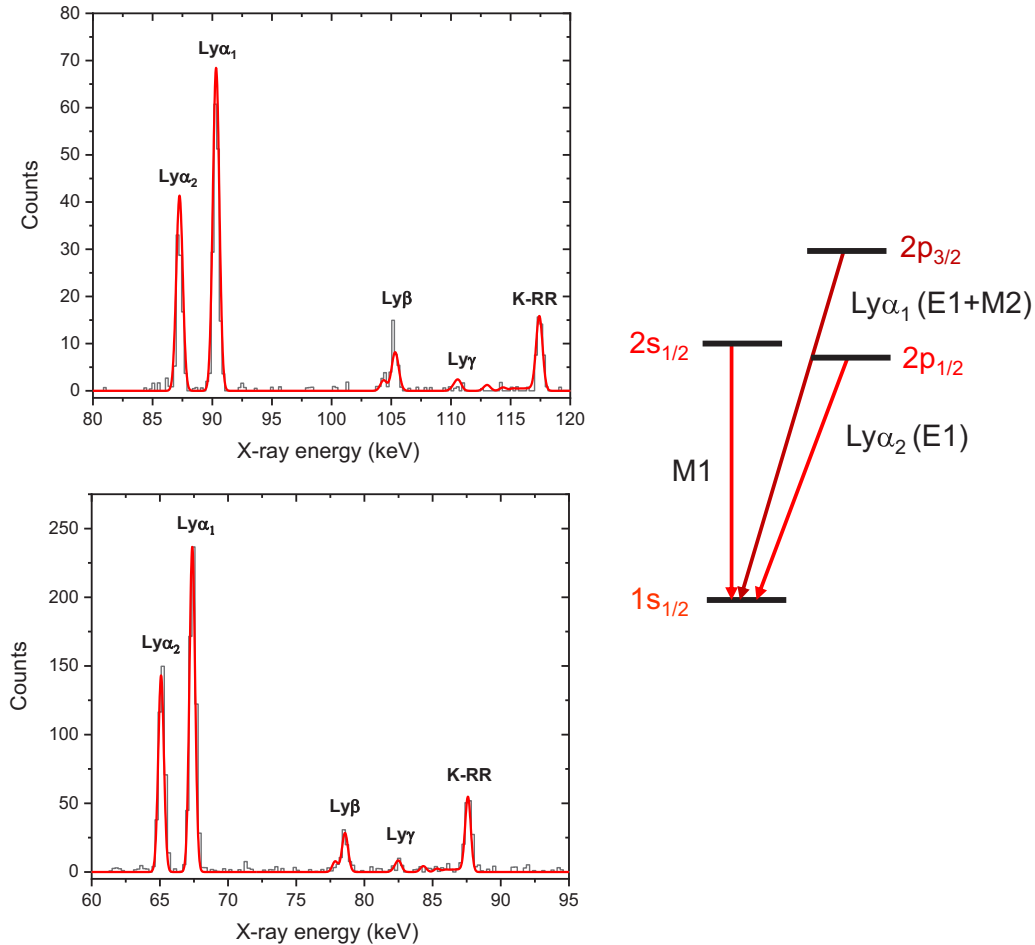


FIG. 6. The Lyman series and the K -RR measured at 0° (top) and 180° (bottom) relative to the ion-beam axis (thin gray lines). The thick red lines display results of the simulation (for details see the text). The intensity of the K -RR line is used for normalization. In the level diagram all possible transition types between the states with $n = 1, 2$ in H-like lead are shown.

Soff [81] as well as from Yerokhin and Shabaev [82] results in an accuracy up to a few eV, and the radiative transition rates are accurate to 99% when compared with tabulated data from Pal'chikov [83].

For high Rydberg states with the main quantum number $n > 100$, a fast computation code [84] was applied for the evaluation of radiative properties in a nonrelativistic approximation. For bound-bound transitions, the technique based on recurrence relations calculating the dipole matrix elements proved to be accurate and stable for values of the main quantum number n up to 500.

IV. RESULTS AND DISCUSSION

As discussed in the previous section, radiative recombination into highly excited states of the projectile will result in decay cascades, mainly by electric dipole transitions, and is likely to end up in one of the intermediate states considered here. While the cascade photons between highly excited levels are usually not detected, the decay photons involving K , L , and M shells are measured by Ge(i) detectors (see Fig. 2). To compare our results with theoretical spectrum modeling, the measured x-ray spectra are corrected for the energy-dependent detection efficiencies of each individual x-ray detector. For

this purpose the germanium detector response function is simulated with the well-established Monte Carlo EGS5 code [85]. For the specific detectors applied, this method has been proven to provide reliable results, in particular for the case of relative (not absolute) detector efficiencies (see, e.g., [86]).

In the following, we concentrate on the discussion of the observed prompt RR transitions as well as of the characteristic x-ray lines in comparison with the simulation based on the theoretical modeling described in Sec. III. In the spectra the very small line broadening of the RR lines due to the temperature of the electron beam is negligible compared to the intrinsic resolution of the detectors. The strongest line associated with the direct RR refers to recombination into the $1s_{1/2}$ ground state (K -RR), and the intensity of other recombination transitions observed drops off as the recombination rates scale approximately as $1/n$ [20,75] for the inner shells. The L -RR populates the excited L -shell levels in Pb^{81+} and hence contributes to the initial line intensity of the $Ly-\alpha_{1,2}$ transition. Likewise, the M -RR contributes to the Balmer series and the $Ly-\beta$ transition.

Figure 6 shows the part of the x-ray spectra containing the Lyman transitions along with the K -RR radiation (laboratory frame; thin gray lines), recorded at the two observation angles of 0° and 180° in comparison with the results of

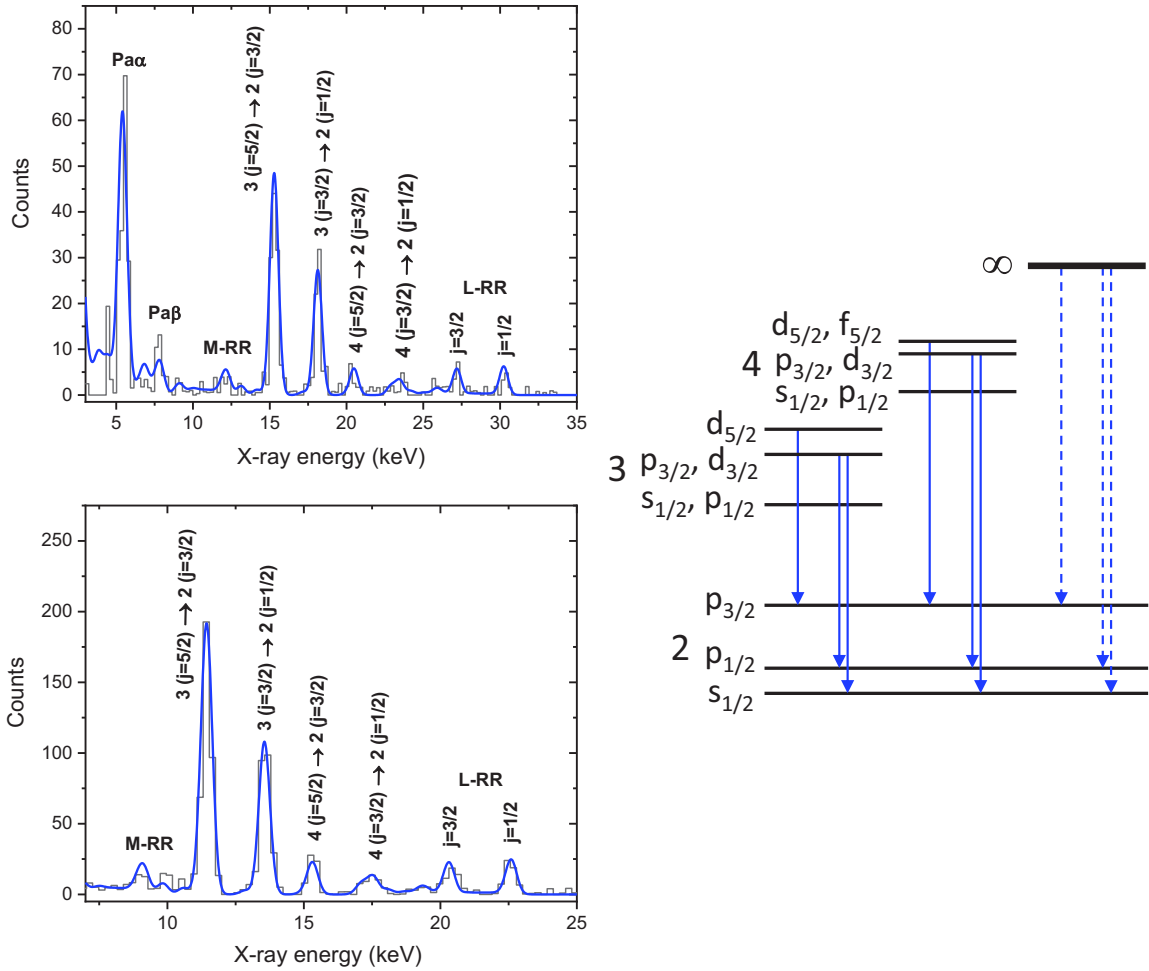


FIG. 7. X-ray spectra associated with prompt *L*-RR and *M*-RR radiation together with characteristic Balmer and Paschen transitions measured by two Ge(i) detectors placed at 0° (top) and 180° (bottom) with respect to the ion-beam axis (thin gray lines). The thick blue lines give the results of the cascade simulation. Two intense Balmer transitions are Balmer- α_1 , $3 (j = 5/2) \rightarrow 2 (j = 3/2)$, and Balmer- α_2 , $3 (j = 3/2) \rightarrow 2 (j = 1/2)$. In the level diagram the Balmer transitions relevant for our measurement are shown.

the spectra simulation (thick red lines). The simulated spectral line profiles are approximated by a Gaussian function with a FWHM of 550 eV to account for the intrinsic resolution of the Ge(i) detectors used. In addition, the experimental spectra displayed have been corrected for the energy-dependent detector (relative) efficiency. The prompt *K*-RR line intensity appearing at an x-ray energy of 101 keV in the projectile frame is used to normalize the simulated Lyman spectrum. For the Ly- α_2 $2p_{1/2} \rightarrow 1s_{1/2}$ transition there is a line blend due to the $2s_{1/2} \rightarrow 1s_{1/2}$ *M*1 decay which is energetically separated from the former by an $n = 2$ Lamb shift of 39 eV [82] which cannot be resolved in our spectra due to the intrinsic detector resolution. Moreover, we note that for Pb^{81+} the *M*1 decay rate amounts to $\Gamma_{M1} = 5.32 \times 10^{13} \text{ s}^{-1}$, whereas the one for the competing two-photon decay channel amounts to $\Gamma_{2E1} = 2.03 \times 10^{12} \text{ s}^{-1}$ [87]. Due to the dominance of the *M*1 decay for the $2s_{1/2}$ state, in the following the two-photon decay is neglected. Based on our spectrum simulation, we estimate that the *M*1 $2s_{1/2} \rightarrow 1s_{1/2}$ ground-state transition contributes about 15% to the observed Ly- α_2 intensity. Overall, very good agreement between the experimental and simulated spectra can be stated for both observation angles.

Complementary information on the Lyman spectrum is provided by the Balmer and Paschen series. In Fig. 7 we compare the experimentally recorded low-energy x-ray spectra (thin gray lines), consisting of the prompt *L*-RR and *M*-RR x-ray transitions together with the characteristic Balmer and Paschen series at 0° and 180°, with our theoretical model based on cascade calculations (thick blue lines). Again, for comparison with the experimental data, the line intensity of the *K*-RR population is used to normalize the simulated spectra. In addition, the most prominent Balmer lines in the spectra are marked by arrows in the level diagram, explaining the origin of various characteristic x-ray lines. Here, we would like to stress that, due to the Doppler blueshift in combination with the high transmission of low-energy photons through the beryllium view port at 0°, Paschen radiation from Pb^{81+} was observed with a relative intensity comparable to the overall line intensities of the Balmer spectrum. However, due to the narrow line spacing, the experimental resolution does not allow us to resolve the individual transitions contributing to the observed Paschen- α line, whereas in the case of the Balmer series, a multitude of transitions, basically due to the fine-structure splitting of the $n = 2$ and $n = 3$ states, are clearly

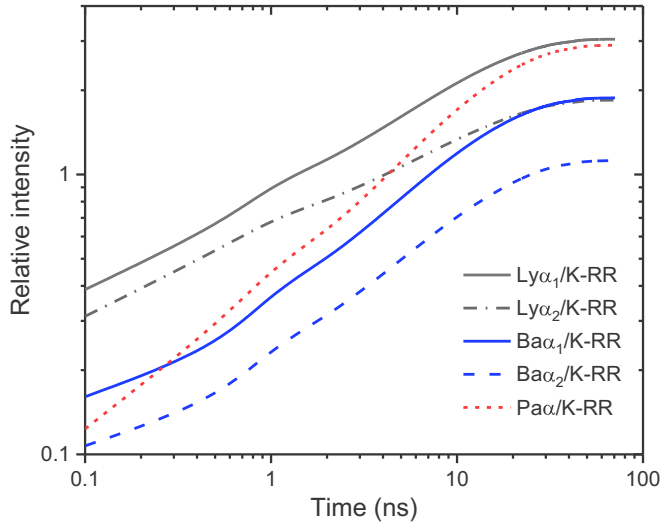


FIG. 8. Cascade calculations of the characteristic line intensities as a function of the flight time of the charge-exchanged Pb^{81+} ions at 10 MeV/u at the electron cooler of the CRYRING@ESR storage ring. All line intensities are normalized to the K -RR population [gray solid (upper) line: $\text{Ly}\alpha_1/K$ -RR; gray dash-dotted line: $\text{Ly}\alpha_2/K$ -RR; blue solid (lower) line: Balmer- α_1/K -RR; blue dashed line: Balmer- α_2/K -RR; red dotted line: Paschen- α/K -RR]. Calculations are performed for recombination into excited projectile states up to $n = 165$.

visible in both x-ray detectors. Only small discrepancies are observed in the region of Paschen lines. These are most likely the result of a low-energy asymmetry of peak profiles that arises from artifacts of the detector and are partially due to the spectrum absorption effects in the beryllium window that are not regarded thoroughly in the low-energy part. Furthermore, the well-resolved L -RR $_{j=3/2}$ and L -RR $_{j=1/2}$ x-ray lines mark at the same time the series limit for transitions decaying from high n levels directly into the $2s_{1/2}$, $2p_{1/2}$, and $2p_{3/2}$ levels.

In contrast to the Balmer series measured at high collision energies where RR favors capture into s states, resulting in $s \rightarrow p$ transitions [76] (e.g., the $3s_{1/2} \rightarrow 2p_{3/2}$), the dominant transitions observed in the current experiment stem from atomic levels with angular momenta $l \geq 1$. This distinct difference is again attributed to the role of the RR population mechanism in which electron capture at low relative energies preferentially populates n states with $l \approx n/3$ [71]. Moreover, so that we can make a comparing with the observed x-ray line emission, the initial (n, l) population distribution is the starting point for cascade calculations based on the specific decay rates of the individual levels to be considered. For the inner shells ($n < 10$), these cascades lead to a preferred population of high angular momentum states with $l = n - 1$, resulting in subsequent yrast transitions with $l \rightarrow l - 1$ [88]. Indeed, the corresponding theoretical x-ray line spectra seem to describe the experimental findings very well (see Figs. 6 and 7).

Since we record in our measurement both the prompt RR transitions and characteristic Lyman, Balmer, and even Paschen series produced to a large extent via RR into high Rydberg states and subsequent cascades, our spectra provide the possibility to study the time development of the men-

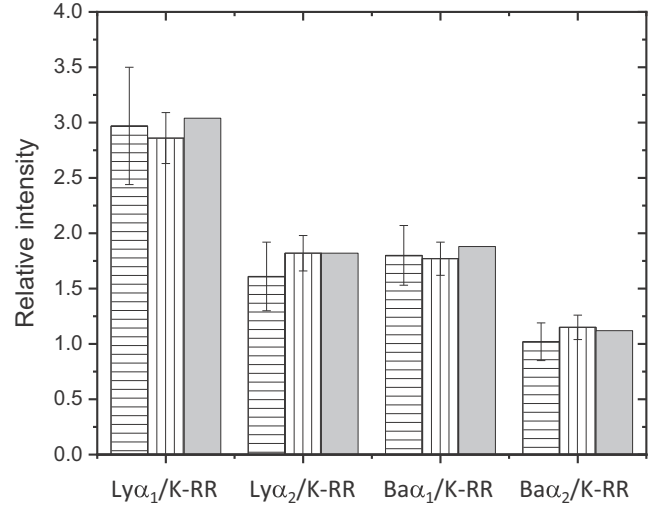


FIG. 9. Experimental results in comparison with the time-dependent theoretical model (gray columns) for characteristic line intensities normalized to that of the K -RR population. White columns with horizontal stripes show experimental data at 0° ; white columns with vertical stripes show experimental data at 180° .

tioned cascade process. The calculated time development of the characteristic line emission is depicted in Fig. 8. In Fig. 8, the characteristic line intensities are normalized to the prompt K -RR intensity. As can be seen, the initial characteristic line intensities induced by direct RR into L and M shells ($t = 0$) are enhanced by up to a factor of 10 following deexcitation cascades within $\Delta t \approx 40$ ns, which is comparable to the time of flight of the ions from the end of cooler section to the dipole magnet in front of the 0° x-ray detector (see Fig. 1). In general, we can state that within this time period, in comparison to the time of flight of the ions inside the cooler section of about 30 ns, the vast majority of electrons having recombined into excited states of the ion reach the ground state. Indeed, the time-integrated line intensities for both detectors appear within statistical accuracy to be in excellent agreement with the results from cascade calculations, as shown in Fig. 9. To underline these findings we present in Table I the experimental ratios of the fine-structure-resolved $\text{Ly}\alpha$ intensities, normalized to the one of the K -RR population in comparison with our theoretical calculations. The L -RR $_{j=3/2,1/2}/K$ -RR intensity ratios should represent the normalized $\text{Ly}\alpha_{1,2}$ intensities at $t = 0$ (prompt x-ray emission) in comparison to

TABLE I. The $\text{Ly}\alpha_1/K$ -RR and $\text{Ly}\alpha_2/K$ -RR ratios obtained for RR into Pb^{82+} in comparison with the time-dependent theoretical model. Corrections to detection efficiencies and angular distributions are applied. Uncertainties shown here are due to counting statistics, whereas systematic uncertainties are neglected.

		0°	180°	Theory
$t \sim 0$ ns	$j = 3/2$	0.287 ± 0.136	0.289 ± 0.061	0.304
	$j = 1/2$	0.338 ± 0.151	0.378 ± 0.072	0.361
$\Delta t \sim 70$ ns	$j = 3/2$	2.965 ± 0.528	2.852 ± 0.229	3.042
	$j = 1/2$	1.613 ± 0.316	1.821 ± 0.156	1.843

the time-integrated one of Ly- $\alpha_{1,2}$ /K-RR ($\Delta t = 70$ ns). Here, we would like to note that for comparison with theory, in Fig. 9 and Table I, the experimental intensity ratios have been corrected for the detection efficiency for both x-ray detectors. It is also important to stress that these findings are generally consistent with those from earlier studies conducted at the ESR electron cooler [15,34,35,55].

Based on the comparison with the observed Ly- α line intensities (see Fig. 9), we conclude that there is a very significant contribution to the Ly- α emission arising from recombination into highly excited states and subsequent cascades: $86.3\% \pm 15.6\%$ for Ly- α_2 and $93.6\% \pm 12\%$ for Ly- α_1 for the 0° detector and $87.4\% \pm 6.5\%$ for Ly- α_2 and $94\% \pm 5.5\%$ for Ly- α_1 at 180° . Also, we would like to point out that within the statistical accuracy reached, the consistent results obtained at 0° and 180° appear to be kind of remarkable because of the very different observation geometries. Whereas the observation at 0° is, in particular, sensitive to delayed emission occurring outside the electron-cooler section, the latter is substantially suppressed at 180° due to the strongly reduced solid angle (see Sec. II). This also confirms the theoretical model applied which predicts that strongly delayed x-ray emission due to recombination into high Rydberg states makes only a very minor contribution to the total recombination rate for the excited states (e.g., recombination into excited states with principal quantum numbers below $n = 100$ contributes 90% to the total rate).

V. SUMMARY AND OUTLOOK

In summary, we have performed an x-ray spectroscopy study of the RR process for bare lead ions at the electron cooler of the CRYRING@ESR storage ring which was recently installed and commissioned at GSI/FAIR. The clearly resolved characteristic projectile x rays together with RR transitions registered at 0° and 180° observation geometry enable us to investigate in detail the prevailing cascade decay dynamics at ultracold cooling conditions. Based on

our elaborate theoretical model, the observed relative intensities of Lyman, Balmer, and Paschen series measured for H-like lead ions were well reproduced, proving that the applied theoretical approaches and, in particular, the rigorous relativistic calculations are an appropriate tool for the state-selective description of recombination at low collision energies. Therefore, this commissioning experiment and well-verified theoretical model will facilitate the future precision x-ray spectroscopy experiments planned at the electron cooler of CRYRING@ESR. In a future run, one may aim to measure the absolute x-ray line intensities, in contrast to intensity ratios as applied in the present study. This could provide state-selective data on the so-called rate enhancement phenomena observed up to now only for total RR rates. In addition, with further decelerated ion-beam energies, we could gain access to longer delay and cascade times and thus to even higher Rydberg states.

ACKNOWLEDGMENTS

The substantial support provided by N. Angert, B. Franzke, R. Maier, and Ö. Skeppstedt to initiate the project CRYRING@ESR is acknowledged. The authors are indebted to the ESR team, M. Steck, S. Litvinov, B. Lorentz, and their colleagues, for providing us with an excellent beam. We wish to thank also S. Bernitt, C.-Y. Chen, and M.-F. Gu for fruitful discussions of the FAC code. This research has been conducted in the framework of the SPARC collaboration, experiment E138 of FAIR Phase-0 supported by GSI. It is further supported by the Extreme Matter Institute EMMI and by the European Research Council (ERC) under the European Union's Horizon 2020 research as well as by the innovation program (Grant No. 682841 "ASTRUM") and Grant Agreement No. 6544002, ENSAR2. B.Z. acknowledges Doctoral Fellowship 2018.9-2022.2 supported by Chinese Scholarship Council (Grant No. 201806180051). We also acknowledge the support provided by ErUM FSP T05 "Aufbau von APPA bei FAIR" (BMBF No. 05P19SJFAA and No. 05P19RGFA1).

-
- [1] L. H. Andersen, J. Bolko, and P. Kvistgaard, Radiative Recombination Between Free Electrons and Bare Carbon Ions, *Phys. Rev. Lett.* **64**, 729 (1990).
 - [2] L. H. Andersen and J. Bolko, Radiative recombination between fully stripped ions and free electrons, *Phys. Rev. A* **42**, 1184 (1990).
 - [3] S. P. Møller, The Aarhus storage ring for ions and electrons ASTRID, in *Proceedings of International Conference on Particle Accelerators* (IEEE, Piscataway, NJ, 1993), pp. 1741–1743.
 - [4] A. Wolf, J. Berger, M. Bock, D. Habs, B. Hochadel, G. Kilgus, G. Neureither, U. Schramm, D. Schwalm, E. Szmola, A. Müller, M. Wagner, and R. Schuch, Experiments with highly-charged ions in the storage ring TSR, *Z. Phys. D* **21**, S69 (1991).
 - [5] G. Gwinner, A. Hoffknecht, T. Bartsch, M. Beutelspacher, N. Eklöv, P. Glans, M. Grieser, S. Krohn, E. Lindroth, A. Müller, A. A. Saghiri, S. Schippers, U. Schramm, D. Schwalm, M. Tokman, G. Wissler, and A. Wolf, Influence of Magnetic Fields on Electron-Ion Recombination at Very Low Energies, *Phys. Rev. Lett.* **84**, 4822 (2000).
 - [6] T. Quinteros, H. Gao, D. R. DeWitt, R. Schuch, M. Pajek, S. Asp, and D. Belkić, Recombination of D^+ and He^+ ions with low-energy free electrons, *Phys. Rev. A* **51**, 1340 (1995).
 - [7] H. Gao, D. R. DeWitt, R. Schuch, W. Zong, S. Asp, and M. Pajek, Observation of Enhanced Electron-Ion Recombination Rates at Very Low Energies, *Phys. Rev. Lett.* **75**, 4381 (1995).
 - [8] E. Lindroth, H. Danared, P. Glans, Z. Pešić, M. Tokman, G. Viktor, and R. Schuch, QED Effects in Cu-Like Pb Recombination Resonances Near Threshold, *Phys. Rev. Lett.* **86**, 5027 (2001).
 - [9] R. Schuch, E. Lindroth, S. Madzunkov, M. Fogle, T. Mohamed, and P. Indelicato, Dielectronic Resonance Method for Measuring Isotope Shifts, *Phys. Rev. Lett.* **95**, 183003 (2005).
 - [10] S. P. Møller, ASTRID—A small multi-purpose storage ring, *3rd European Particle Accelerator Conference* (CERN, 1992), p. 158.
 - [11] R. Schuch, A. Bárány, H. Danared, N. Elander, and S. Mannervik, Storage rings, a new tool for atomic physics, *Nucl. Instrum. Methods Phys. Res., Sect. B* **43**, 411 (1989).

- [12] D. Habs, W. Baumann, J. Berger, P. Blatt, A. Faulstich, P. Krause, G. Kilgus, R. Neumann, W. Petrich, R. Stokstad *et al.*, First experiments with the Heidelberg test storage ring TSR, *Nucl. Instrum. Methods Phys. Res., Sect. B* **43**, 390 (1989).
- [13] A. Hoffknecht, C. Brandau, T. Bartsch, C. Böhme, H. Knopp, S. Schippers, A. Müller, C. Kozhuharov, K. Beckert, F. Bosch, B. Franzke, A. Krämer, P. H. Mokler, F. Nolden, M. Steck, Th. Stöhlker, and Z. Stachura, Recombination of bare Bi⁸³⁺ ions with electrons, *Phys. Rev. A* **63**, 012702 (2000).
- [14] W. Shi, S. Böhm, C. Böhme, C. Brandau, A. Hoffknecht, S. Kieslich, S. Schippers, A. Müller, C. Kozhuharov, F. Bosch *et al.*, Recombination of U⁹²⁺ ions with electrons, *Eur. Phys. J. D* **15**, 145 (2001).
- [15] R. Reuschl, A. Gumberidze, C. Kozhuharov, U. Spillmann, S. Tashenov, Th. Stöhlker, and J. Eichler, State-selective x-ray studies of radiative recombination into bare and H-like uranium at threshold energies, *Phys. Rev. A* **77**, 032701 (2008).
- [16] D. Banaś *et al.*, Subshell-selective x-ray studies of radiative recombination of U⁹²⁺ ions with electrons for very low relative energies, *Phys. Rev. A* **92**, 032710 (2015).
- [17] R. E. Marrs, S. R. Elliott, and D. A. Knapp, Production and Trapping of Hydrogenlike and Bare Uranium Ions in an Electron Beam Ion Trap, *Phys. Rev. Lett.* **72**, 4082 (1994).
- [18] R. E. Marrs, P. Beiersdorfer, S. R. Elliott, D. A. Knapp, and Th. Stöhlker, The super electron beam ion trap, *Phys. Scr.* **T59**, 183 (1995).
- [19] J. Eichler and Th. Stöhlker, Radiative electron capture in relativistic ion-atom collisions and the photoelectric effect in hydrogen-like high-Z systems, *Phys. Rep.* **439**, 1 (2007).
- [20] H. A. Kramers, XCIII. On the theory of x-ray absorption and of the continuous x-ray spectrum, *London, Edinburgh Dublin Philos. Mag. J. Sci.* **46**, 836 (1923).
- [21] M. Stobbe, Zur quantenmechanik photoelektrischer prozesse, *Ann. Phys. (Berlin, Ger.)* **399**, 661 (1930).
- [22] A. Ichihara, T. Shirai, and J. Eichler, Radiative electron capture in relativistic atomic collisions, *Phys. Rev. A* **49**, 1875 (1994).
- [23] J. Eichler, A. Ichihara, and T. Shirai, Alignment caused by photoionization and in radiative electron capture into excited states of hydrogenic high-Z ions, *Phys. Rev. A* **58**, 2128 (1998).
- [24] A. Surzhykov, S. Fritzsche, Th. Stöhlker, and S. Tashenov, Polarization studies on the radiative recombination of highly charged bare ions, *Phys. Rev. A* **68**, 022710 (2003).
- [25] J. H. Scofield, Angular distribution of cascade x-rays following radiative recombination from a beam, *Phys. Rev. A* **44**, 139 (1991).
- [26] S. Fritzsche, A. Surzhykov, and Th. Stöhlker, Radiative recombination into high-Z few-electron ions: Cross sections and angular distributions, *Phys. Rev. A* **72**, 012704 (2005).
- [27] V. M. Shabaev, V. A. Yerokhin, T. Beier, and J. Eichler, QED corrections to the radiative recombination of an electron with a bare nucleus, *Phys. Rev. A* **61**, 052112 (2000).
- [28] J. Holmberg, A. N. Artemyev, A. Surzhykov, V. A. Yerokhin, and Th. Stöhlker, QED corrections to radiative recombination and radiative decay of heavy hydrogenlike ions, *Phys. Rev. A* **92**, 042510 (2015).
- [29] J. Eichler and A. Ichihara, Polarization of photons emitted in radiative electron capture by bare high-Z ions, *Phys. Rev. A* **65**, 052716 (2002).
- [30] A. Surzhykov, S. Fritzsche, and Th. Stöhlker, Polarization of the Lyman- α_1 line following the radiative recombination of bare, high-Z ions, *Hyperfine Interact.* **146**, 35 (2003).
- [31] J. Eichler, A. Ichihara, and T. Shirai, Photon angular distributions from radiative electron capture in relativistic atomic collisions, *Phys. Rev. A* **51**, 3027 (1995).
- [32] A. E. Klasnikov, A. N. Artemyev, T. Beier, J. Eichler, V. M. Shabaev, and V. A. Yerokhin, Spin-flip process in radiative recombination of an electron with H- and Li-like uranium, *Phys. Rev. A* **66**, 042711 (2002).
- [33] A. Müller, S. Schennach, M. Wagner, J. Haselbauer, O. Uwira, W. Spies, E. Jennewein, R. Becker, M. Kleinod, U. Pröbstel *et al.*, Recombination of free electrons with ions, *Phys. Scr.* **T37**, 62 (1991).
- [34] H. F. Beyer, D. Liesen, F. Bosch, K. D. Finlayson, M. Jung, O. Klepper, R. Moshhammer, K. Beckert, H. Eickhoff, B. Franzke *et al.*, X-rays from radiative electron capture of free cooling electrons for precise Lamb-shift measurements at high Z: Au⁷⁸⁺, *Phys. Lett. A* **184**, 435 (1994).
- [35] D. Liesen, H. F. Beyer, K. D. Finlayson, F. Bosch, M. Jung, O. Klepper, R. Moshhammer, K. Beckert, H. Eickhoff, B. Franzke *et al.*, X-rays from radiative electron capture of highly-charged heavy ions in an electron cooler, *Z. Phys. D* **30**, 307 (1994).
- [36] H. F. Beyer, G. Menzel, D. Liesen, A. Gallus, F. Bosch, R. Deslattes, P. Indelicato, Th. Stöhlker, O. Klepper, R. Moshhammer *et al.*, Measurement of the ground-state Lamb shift of hydrogenlike uranium at the electron cooler of the ESR, *Z. Phys. D* **35**, 169 (1995).
- [37] A. Gumberidze, Th. Stöhlker, D. Banaś, K. Beckert, P. Beller, H. F. Beyer, F. Bosch, X. Cai, S. Hagmann, C. Kozhuharov, D. Liesen, F. Nolden, X. Ma, P. H. Mokler, A. Oršić-Muthig, M. Steck, D. Sierpowski, S. Tashenov, A. Warczak, and Y. Zou, Electron-Electron Interaction in Strong Electromagnetic Fields: The Two-Electron Contribution to the Ground-State Energy in He-Like Uranium, *Phys. Rev. Lett.* **92**, 203004 (2004).
- [38] A. Gumberidze, Th. Stöhlker, D. Banaś, K. Beckert, P. Beller, H. F. Beyer, F. Bosch, S. Hagmann, C. Kozhuharov, D. Liesen, F. Nolden, X. Ma, P. H. Mokler, M. Steck, D. Sierpowski, and S. Tashenov, Quantum Electrodynamics in Strong Electric Fields: The Ground-State Lamb Shift in Hydrogenlike Uranium, *Phys. Rev. Lett.* **94**, 223001 (2005).
- [39] P. H. Mokler, Th. Stöhlker, C. Kozhuharov, R. Moshhammer, P. Rymuza, F. Bosch, and T. Kandler, Structure of very heavy few-electron ions—new results from the heavy ion storage ring, ESR, *Phys. Scr.* **T51**, 28 (1994).
- [40] R. Marrus and P. J. Mohr, Forbidden transitions in one- and two-electron atoms, *Adv. At. Mol. Phys.* **14**, 181 (1979).
- [41] O. Jitrik and C. F. Bunge, Salient features of electric and magnetic multipole transition probabilities of hydrogen-like systems, *Phys. Scr.* **69**, 196 (2004).
- [42] M. Durante, P. Indelicato, B. Jonson, V. Koch, K. Langanke, U.-G. Meißner, E. Nappi, T. Nilsson, Th. Stöhlker, E. Widmann *et al.*, All the fun of the FAIR: fundamental physics at the facility for antiproton and ion research, *Phys. Scr.* **94**, 033001 (2019).
- [43] H. Danared *et al.*, Stockholm University, Technical design report: LSR Low-energy Storage Ring, 2011 (unpublished), https://fair-center.eu/fileadmin/FAIR/publications_exp/DesignReportLSR_1.3.pdf.

- [44] Th. Stöhlker, V. Bagnoud, K. Blaum, A. Blazevic, A. Bräuning-Demian, M. Durante, F. Herfurth, M. Lestinsky, Y. Litvinov, S. Neff *et al.*, APPA at FAIR: From fundamental to applied research, *Nucl. Instrum. Methods Phys. Res., Sect. B* **365**, 680 (2015).
- [45] M. Lestinsky, V. Andrianov, B. Aurand, V. Bagnoud, D. Bernhardt, H. Beyer, S. Bishop, K. Blaum, A. Bleile, At. Borovik Jr. *et al.*, Physics book: CRYRING@ESR, *Eur. Phys. J.: Spec. Top.* **225**, 797 (2016).
- [46] H. Danared, G. Andler, L. Bagge, C. Herrlander, J. Hilke, J. Jeansson, A. Källberg, A. Nilsson, A. Paál, K.-G. Rensfelt, U. Rosengard, J. Starker, and M. af Ugglas, Electron Cooling with an Ultracold Electron Beam, *Phys. Rev. Lett.* **72**, 3775 (1994).
- [47] H. Danared, A. Källberg, G. Andler, L. Bagge, F. Österdahl, A. Paál, K.-G. Rensfelt, A. Simonsson, Ö. Skeppstedt, and M. Af Ugglas, Studies of electron cooling with a highly expanded electron beam, *Nucl. Instrum. Methods Phys. Res., Sect. A* **441**, 123 (2000).
- [48] Th. Stöhlker, Y. A. Litvinov, A. Bräuning-Demian, M. Lestinsky, F. Herfurth, R. Maier, D. Prasuhn, R. Schuch, and M. Steck, SPARC collaboration: New strategy for storage ring physics at FAIR, *Hyperfine Interact.* **227**, 45 (2014).
- [49] C. Pies, S. Schäfer, S. Heuser, S. Kempf, A. Pabinger, J.-P. Porst, P. Ranitsch, N. Foerster, D. Hengstler, A. Kampkötter *et al.*, maXS: Microcalorimeter arrays for high-resolution x-ray spectroscopy at GSI/FAIR, *J. Low Temp. Phys.* **167**, 269 (2012).
- [50] D. Hengstler, M. Keller, C. Schötz, J. Geist, M. Krantz, S. Kempf, L. Gastaldo, A. Fleischmann, T. Gassner, G. Weber *et al.*, Towards FAIR: first measurements of metallic magnetic calorimeters for high-resolution x-ray spectroscopy at GSI, *Phys. Scr.* **T166**, 014054 (2015).
- [51] H. Poth, Electron cooling: Theory, experiment, application, *Phys. Rep.* **196**, 135 (1990).
- [52] F. M. Kröger, G. Weber, O. Forstner, A. Gumberidze, M. O. Herdrich, M. Lestinsky, A. Kalinin, Th. Köhler, E. B. Menz, Ph. Pfäfflein, U. Spillmann, and Th. Stöhlker, New setup for x-ray spectroscopy at the CRYRING@ESR electron cooler, *Helmholtz Inst. Jena Annu. Rep.* **2019**, 45 (2020).
- [53] R. Schuch, H. Poth, and A. Wolf, X-ray measurements at the stand-alone electron cooler for LEAR, *Nucl. Instrum. Methods Phys. Res., Sect. A* **276**, 445 (1989).
- [54] Z. Andelkovic *et al.*, Facility for Antiproton and Ion Research, Technical design report: Experimental Instrumentation of CRYRING@ESR, 2018 (unpublished), https://www.gsi.de/fileadmin/Atomphysik/Sparc/Technical_Design_Report_CRYRING_Instrumentation.pdf.
- [55] M. Pajek and R. Schuch, X-rays from recombination of bare ions with electrons in an electron cooler, *Nucl. Instrum. Methods Phys. Res., Sect. B* **98**, 165 (1995).
- [56] A. Müller, D. S. Belić, B. D. DePaola, N. Djurić, G. H. Dunn, D. W. Mueller, and C. Timmer, Experimental measurements of field effects on dielectronic recombination cross sections and Rydberg product-state distributions, *Phys. Rev. A* **36**, 599 (1987).
- [57] W. Zong, R. Schuch, H. Gao, D. R. DeWitt, and N. R. Badnell, Low-energy recombination of Ne^{7+} , *J. Phys. B.* **31**, 3729 (1998).
- [58] R. Schuch, W. Zong, and N. R. Badnell, Recombination of cooled highly charged ions with low-energy electrons, *Int. J. Mass Spectrom.* **192**, 225 (1999).
- [59] C. Biedermann, H. Gao, R. Schuch, W. Zong, S. Asp, D. R. DeWitt, and H. Kuiper, Study of radiative recombination into deuterium Rydberg states, *J. Phys. B* **28**, 505 (1995).
- [60] S. Schippers, A. Müller, G. Gwinner, J. Linkemann, A. A. Saghir, and A. Wolf, Storage ring measurement of the C IV recombination rate coefficient, *Astrophys. J.* **555**, 1027 (2001).
- [61] S. Böhm, S. Schippers, W. Shi, A. Müller, N. Eklöv, R. Schuch, H. Danared, N. R. Badnell, D. M. Mitnik, and D. C. Griffin, Measurement of the field-induced dielectronic-recombination-rate enhancement of O^{5+} ions differential in the Rydberg quantum number n , *Phys. Rev. A* **65**, 052728 (2002).
- [62] H. F. Beyer, O. Guzman, and D. Liesen, On the total recombination between cooling electrons and heavy ions, *Part. Accel.* **24**, 163 (1989).
- [63] M. Pajek and R. Schuch, Plasma effects in three-body recombination of high-Z bare ions with electrons, *Phys. Scr.* **T80**, 307 (1999).
- [64] O. Brinzaescu, J. Eichler, A. Ichihara, T. Shirai, and Th. Stöhlker, Comparison between the nonrelativistic dipole approximation and the exact relativistic theory for radiative recombination, *Phys. Scr.* **T80**, 324 (1999).
- [65] R. H. Pratt, A. Ron, and H. K. Tseng, Atomic photoelectric effect above 10 keV, *Rev. Mod. Phys.* **45**, 273 (1973).
- [66] A. Ichihara and J. Eichler, Cross sections for radiative recombination and the photoelectric effect in the K, L, and M shells of one-electron systems with $1 \leq Z \leq 112$ calculated within an exact relativistic description, *At. Data Nucl. Data Tables* **74**, 1 (2000).
- [67] H. A. Bethe and E. E. Salpeter, *Quantum Mechanics of One- and Two-Electron Atoms* (Springer, Berlin, 1957).
- [68] A. Burgess and M. J. Seaton, A general formula for the calculation of atomic photo-ionization cross sections, *Mon. Notices R. Astron. Soc.* **120**, 121 (1960).
- [69] A. Burgess, Tables of hydrogenic photoionization cross-sections and recombination coefficients, *Mem. R. Astron. Soc.* **69**, 1 (1965).
- [70] O. Brinzaescu and Th. Stöhlker, Radiative recombination rate coefficients, *Phys. Scr.* **T92**, 275 (2001).
- [71] M. Pajek and R. Schuch, Radiative recombination of bare ions with low-energy free electrons, *Phys. Rev. A* **45**, 7894 (1992).
- [72] E. B. Menz, M. Lestinsky, S. Fuchs, W. Biela-Nowaczyk, A. Borovik, Jr., C. Brandau, S. Schippers, and Th. Stöhlker, First DR experiment at CRYRING@ESR, *Helmholtz Inst. Jena Annu. Rep.* **2020**, 55 (2021).
- [73] R. Schuch, W. Zong, W. Spies, P. Glans, and H. Danared, A first study of dielectronic recombination with the super-expanded electron beam in CRYRING, *Hyperfine Interact.* **115**, 123 (1998).
- [74] S. Böhm, A. Müller, S. Schippers, W. Shi, M. Fogle, P. Glans, R. Schuch, and H. Danared, Experimental N V and Ne VIII low-temperature dielectronic recombination rate coefficients, *Astron. Astrophys.* **437**, 1151 (2005).
- [75] H. Gao, E. Justiniano, S. Asp, H. Danared, D. R. DeWitt, and R. Schuch, Role of electron-ion recombination processes in the lifetime of stored D^+ beams, *Phys. Rev. A* **54**, 3005 (1996).

- [76] Th. Stöhlker, F. Bosch, A. Gallus, C. Kozhuharov, G. Menzel, P. H. Mokler, H. T. Prinz, J. Eichler, A. Ichihara, T. Shirai, R. W. Dunford, T. Ludziejewski, P. Rymuza, Z. Stachura, P. Swiat, and A. Warczak, Strong Alignment Observed for the Time-Reversed Photoionization Process Studied in Relativistic Collisions with Bare Uranium Ions, *Phys. Rev. Lett.* **79**, 3270 (1997).
- [77] A. Ichihara and J. Eichler, Angle-differential cross sections for radiative recombination and the photoelectric effect in the K, L, and M shells of one-electron systems calculated within an exact relativistic description, *At. Data Nucl. Data Tables* **79**, 187 (2001).
- [78] J. Eichler, Angular distribution of de-excitation x-rays from radiative electron capture in relativistic atomic collisions, *Nucl. Phys. A* **572**, 147 (1994).
- [79] M. F. Gu, Indirect x-ray line-formation processes in iron L-shell ions, *Astrophys. J.* **582**, 1241 (2003).
- [80] M. F. Gu, The flexible atomic code, *Can. J. Phys.* **86**, 675 (2008).
- [81] W. R. Johnson and G. Soff, The Lamb shift in hydrogen-like atoms, $1 \leq Z \leq 110$, *At. Data Nucl. Data Tables* **33**, 405 (1985).
- [82] V. A. Yerokhin and V. M. Shabaev, Lamb shift of $n = 1$ and $n = 2$ states of hydrogen-like atoms, $1 \leq Z \leq 110$, *J. Phys. Chem. Ref. Data* **44**, 033103 (2015).
- [83] V. G. Pal'chikov, Relativistic transition probabilities and oscillator strengths in hydrogen-like atoms, *Phys. Scr.* **57**, 581 (1998).
- [84] P. J. Storey and D. G. Hummer, Fast computer evaluation of radiative properties of hydrogenic systems, *Comput. Phys. Commun.* **66**, 129 (1991).
- [85] H. Hirayama, Y. Namito, W. R. Nelson, A. F. Bielajew, S. J. Wilderman, and U. Michigan, *The EGS5 Code System* (U.S. Department of Energy, Washington, DC, 2005).
- [86] D. Banaś *et al.*, Two-photon energy distribution from the decay of the 2^1S_0 state in He-like uranium, *Phys. Rev. A* **87**, 062510 (2013).
- [87] F. A. Parpia and W. R. Johnson, Radiative decay rates of metastable one-electron atoms, *Phys. Rev. A* **26**, 1142 (1982).
- [88] R. Reuschl, A. Gumberidze, Th. Stöhlker, C. Kozhuharov, J. Rzadkiewicz, U. Spillmann, S. Tashenov, S. Fritzsche, and A. Surzhykov, The Balmer spectrum of H-like uranium produced by radiative recombination at low velocities, *Radiat. Phys. Chem.* **75**, 1740 (2006).